

A Discontinuous Galerkin Method for Plasma Dynamic Simulations: The Full Two-Fluid System

John Loverich and Uri Shumlak

University of Washington
Department of Aeronautics and Astronautics

American Physical Society
47th Annual Meeting of the Division of Plasma Physics
Denver, Colorado, October 24-28, 2005

URL <http://www.aa.washington.edu/cfdlab>
email: jlovric@u.washington.edu

Abstract

An algorithm for simulation of plasma dynamics using the discontinuous Galerkin method is presented along with results. The algorithm works in multiple dimensions arbitrary geometries and on parallel platforms. The algorithm uses a second or third order genuinely multi-dimensional spatial discretization with 3rd or 4th order time discretizations. Results from the GEM challenge magnetic reconnection problem are presented. Full two-fluid simulations of a Z-pinch are also presented along with the discussion of a fast growing sausage mode (possibly the drift sausage instability) which is accompanied by ion shocks that develop when the electron drift speed is greater than the ion sound speed; this condition is achieved in thin current sheets smaller than a few ion Larmor radii in thickness.

Full Two-Fluid Model: Maxwell's Equations

The two-fluid plasma model consists of a set of fluid equations for the electrons and ions plus the complete Maxwell's equations including displacement current,

$$\partial_t \bar{E} - c^2 (\nabla \times \bar{B}) = -\frac{1}{\epsilon_0} \sum_s \frac{q_s}{m_s} \rho_s \bar{U}_s, \quad (1)$$

$$\partial_t \bar{B} + (\nabla \times \bar{E}) = 0. \quad (2)$$

$$\nabla \cdot \bar{B} = 0 \quad (3)$$

$$\nabla \cdot \bar{E} = \frac{1}{\epsilon_0} (q_i n_i + q_e n_e) \quad (4)$$

Equations (3) and (4) are constraint equations which can be derived from Ampere's law (1) and Faraday's law (2). Equations (3) and (4) are not solved numerically, but they should be watched carefully as errors in these equations can cause serious problems[4].

Full Two-Fluid Model: Fluid Equations

Electrons and ions have separate energy,

$$\partial_t e_s + \nabla \cdot (\bar{U}_s (e_s + P_s)) = \frac{q_s}{m_s} \rho_s \bar{E} \cdot \bar{U}_s ,$$

momentum,

$$\partial_t \rho_s \bar{U}_s + \nabla_\alpha (\rho_s \bar{U}_s^\alpha \bar{U}_s) + \nabla_\alpha (\delta^{\alpha\beta} P_s) = \frac{q_s}{m_s} \rho_s (\bar{E} + \bar{U}_s \times \bar{B}) ,$$

and continuity,

$$\partial_t \rho_s + \nabla \cdot (\rho_s \bar{U}_s) = 0 .$$

so each species has its own temperature, velocity and number density. As a result, quasi-neutrality is not assumed and things like electron plasma waves double layers, and ion current should be observed numerically.

Full Two-Fluid Model: Balance Form

This set of equations can be written as three systems of balance laws,

$$\frac{\partial Q_e}{\partial t} + \nabla \cdot F_e(Q) = \psi_e, \quad (5)$$

for the electron fluid equations,

$$\frac{\partial Q_i}{\partial t} + \nabla \cdot F_i(Q) = \psi_i, \quad (6)$$

for the ion fluid equations, and

$$\frac{\partial Q_{em}}{\partial t} + \nabla \cdot F_{em}(Q) = \psi_{em}, \quad (7)$$

for Maxwell's field equations.

Full Two-Fluid Model: Balance Form

For clarity, these balance laws Eqns.(5)-(7) are given in full form by,

$$\frac{\partial}{\partial t} \begin{pmatrix} \rho_s \\ \rho_s U_{xs} \\ \rho_s U_{ys} \\ \rho_s U_{zs} \\ e_s \end{pmatrix} + \nabla \cdot \begin{pmatrix} \rho_s U_{xs} & \rho_s U_{ys} & \rho_s U_{zs} \\ \rho_s U_{xs} U_{xs} + P_s & \rho_s U_{xs} U_{ys} & \rho_s U_{xs} U_{zs} \\ \rho_s U_{ys} U_{xs} & \rho_s U_{ys} U_{ys} + P_s & \rho_s U_{ys} U_{zs} \\ \rho_s U_{zs} U_{xs} & \rho_s U_{zs} U_{ys} & \rho_s U_{zs} U_{zs} + P_s \\ U_{xs} (e_s + P_s) & U_{ys} (e_s + P_s) & U_{zs} (e_s + P_s) \end{pmatrix} = \begin{pmatrix} 0 \\ q_s n_s (E_x + U_{ys} B_z - U_{zs} B_y) \\ q_s n_s (E_y + U_{zs} B_x - U_{xs} B_z) \\ q_s n_s (E_z + U_{xs} B_y - U_{ys} B_x) \\ q_s n_s (E_x U_{xs} + E_y U_{ys} + E_z U_{zs}) \end{pmatrix}$$

$$\frac{\partial}{\partial t} \begin{pmatrix} B_x \\ B_y \\ B_z \\ E_x \\ E_y \\ E_z \end{pmatrix} + \nabla \cdot \begin{pmatrix} 0 & E_z & -E_y \\ -E_z & 0 & E_x \\ E_y & -E_x & 0 \\ 0 & -c^2 B_z & c^2 B_y \\ c^2 B_z & 0 & -c^2 B_x \\ -c^2 B_y & c^2 B_x & 0 \end{pmatrix} = \begin{pmatrix} 0 \\ 0 \\ 0 \\ -\frac{1}{\epsilon_0} (q_e n_e U_{xe} + q_i n_i U_{xi}) \\ -\frac{1}{\epsilon_0} (q_e n_e U_{ye} + q_i n_i U_{yi}) \\ -\frac{1}{\epsilon_0} (q_e n_e U_{ze} + q_i n_i U_{zi}) \end{pmatrix}$$

Discontinuous Galerkin Method

Discontinuous Galerkin methods are high order extensions of upwind schemes using a finite element formulation where the elements are discontinuous at cell interfaces. Details of the method are discussed in [3] and reproduced here for our particular case. The balance law,

$$\frac{\partial Q}{\partial t} + \nabla \cdot F = \psi ,$$

is multiplied by the set of basis functions $\{v_r\}$ and integrated over the finite volume element K . For second order spatial accuracy the basis set $\{v_r\} = \{v_0, v_x, v_y\} = \{1, \frac{x-x_{ij}}{\frac{1}{2}\Delta x}, \frac{y-y_{ij}}{\frac{1}{2}\Delta y}\}$ is used. The equation is written,

$$\int \frac{\partial Q}{\partial t} v_r dV + \int (\nabla \cdot F) v_r dV = \int \psi v_r dV .$$

Discontinuous Galerkin Method

Integrate by parts to get

$$\int_K \frac{\partial Q}{\partial t} v_r dV + \int_{\partial K} (F \cdot n) v_r d\Gamma - \int_K F \cdot (\nabla v_r) dV = \int_K \psi v_r dV .$$

The discrete conserved variable Q is defined as a linear combination of the basis

functions inside an element K , $Q = Q_0 + v_x Q_x + v_y Q_y$. The integral

$\int_K \frac{\partial Q}{\partial t} v_r dV = \frac{\partial Q_r}{\partial t} C V$ where C is the constant $\frac{1}{V} \int_K v_r^2 dV$ and V is the volume of the element. Using these definitions we get the discrete equation

$$\frac{\partial Q_r}{\partial t} C V + \sum_e \sum_l r_l (F \cdot n) v_r \Gamma_e - \sum_m w_m F \cdot (\nabla v_r) V = \sum_m w_m \psi v_r V ,$$

when the integrals are replaced by appropriate Gaussian quadratures. Γ_e is the surface area of the cell face in consideration, e refers to an element face, r_l are quadrature points on a face and w_m are quadrature points in the volume.

Discontinuous Galerkin Method

The discrete equations for the second order scheme are

$$\frac{\partial Q_0}{\partial t} V + \sum_e \sum_l r_l (F \cdot n) v_0 \Gamma_e = \sum_m w_m \psi v_0 V ,$$

$$\frac{\partial Q_x}{\partial t} V + 3 \sum_e \sum_l r_l (F \cdot n) v_x \Gamma_e - 3 \sum_m w_m F \cdot (\nabla v_x) V = 3 \sum_m w_m \psi v_x V ,$$

$$\frac{\partial Q_y}{\partial t} V + 3 \sum_e \sum_l r_l (F \cdot n) v_y \Gamma_e - 3 \sum_m w_m F \cdot (\nabla v_y) V = 3 \sum_m w_m \psi v_y V .$$

The derivatives of the basis functions can be calculated analytically since the polynomial basis functions are known. The discontinuous Galerkin method is applied to each balance law (5)(6)(7) at every time step. In [2] TVD Runge-Kutta time integration is suggested, though standard Runge-Kutta methods work well. In this paper we use a 3rd order TVD Runge-Kutta scheme as in [2].

High β Collisionless Magnetic Reconnection: GEM Challenge

In ideal MHD the fluid is frozen to the magnetic field lines and so field lines cannot reconnect without some non-ideal term. Resistivity allows field lines to reconnect though much slower than the fast reconnection that occurs in collisionless space and fusion plasmas. This fast reconnection requires at least the addition of the Hall term though electron dissipation occurs through electron inertia effects - this requires two-fluid effects. The simulation is initialized using a Harris current sheet with initial conditions identical to those presented in the GEM challenge papers [1].

High β Collisionless Magnetic Reconnection: In Plane Current

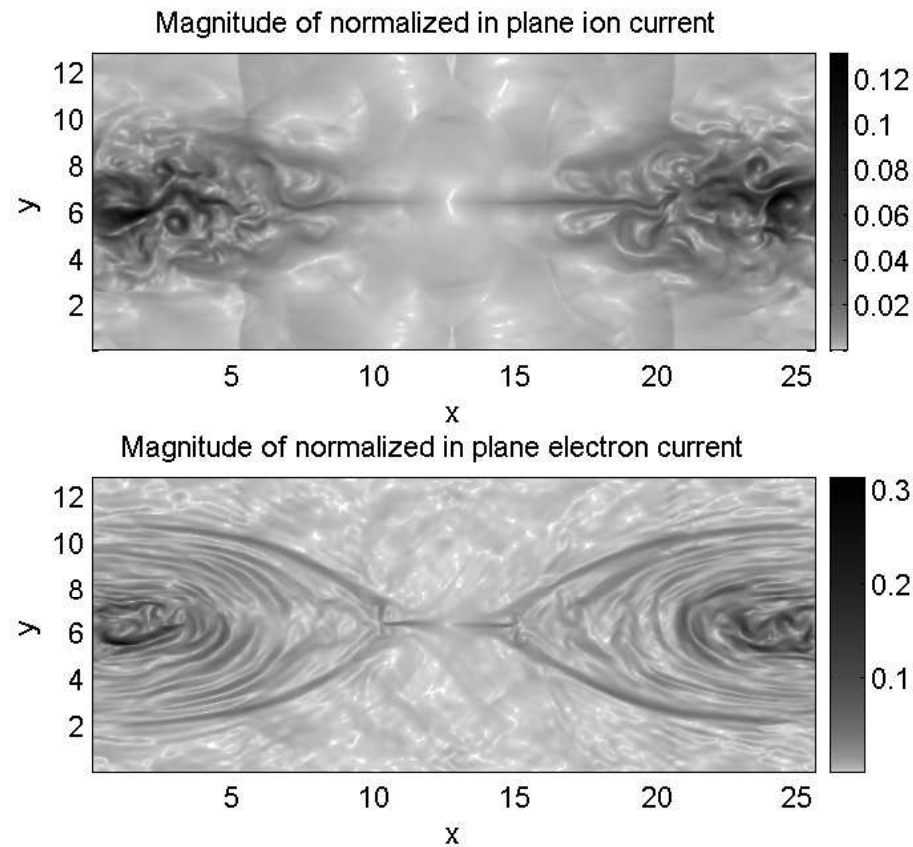


Figure 1: Magnitude of in plane current in the GEM challenge problem after $t = 40/\omega_{ci}$. The electron and ion currents differ substantially in structure because the electrons are frozen to the field lines over a greater range than the ions.

High β Collisionless Magnetic Reconnection

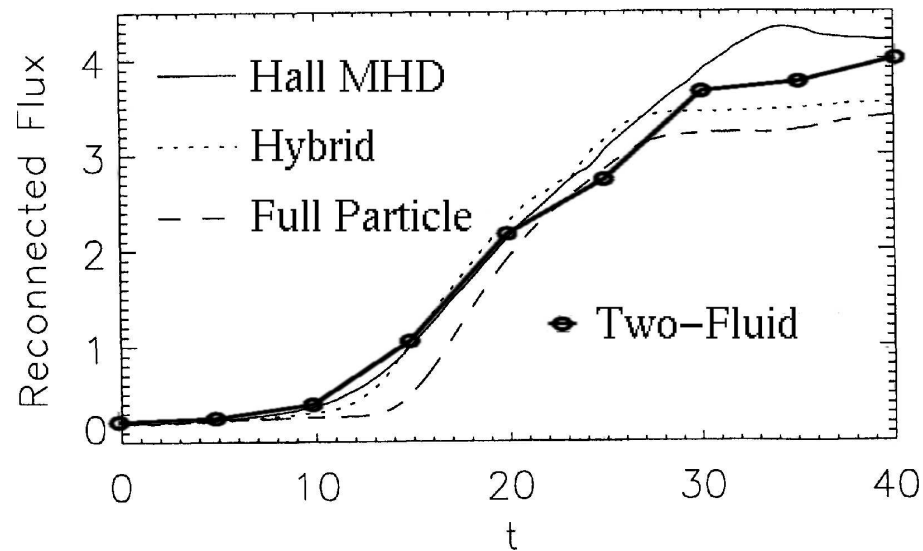


Figure 2: Plot taken from [5] with the two-fluid solution calculated by the authors superimposed on top. Plot of reconnected magnetic flux vs time in units of inverse ω_{c_i} for several published solutions and the two-fluid solution calculated by the authors.

Full Two-Fluid Axisymmetric Z-Pinch

In the following slides, an axisymmetric version of the algorithm is used to evolve axisymmetric two-fluid instabilities in the Z-Pinch. Simulations are run using 2 different pinch radii, $2.5R_{gi}$ and $12.5R_{gi}$ where R_{gi} is the ion Larmor radius. Sinusoidal perturbation in the magnetic field along the axis are used to initialize the instabilities. The solution is initialized using an MHD equilibrium with constant current carried by the electrons. The ion to electron mass ratio is 100. The electron and ion temperatures are initially constant throughout the domain, the electron pressure equals the ion pressure and the electron number density equals the ion number density. A background density and pressure of 10% is added to prevent negative pressures.

Full Two-Fluid Axisymmetric Z-Pinch

Pinch radius $R = 12.5 R_{gi}$

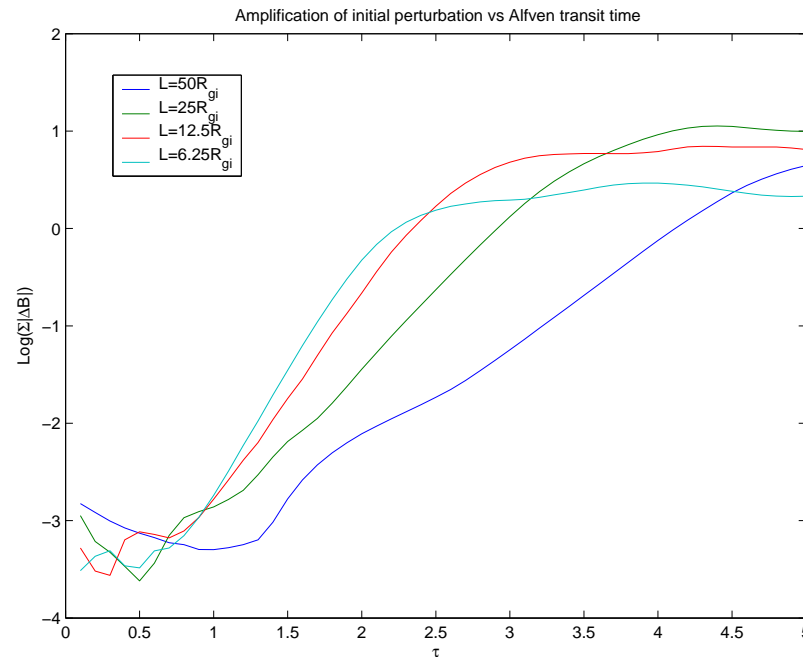


Figure 3: Plots of the growth in the perturbed magnetic field vs time normalized by the Alfvén transit time across the radius. The Z-pinch has radius $R = 12.5 R_{gi}$ and plots are shown for various wavelength perturbations L . The growth occurs on MHD time scales as expected for the sausage instability.

Full Two-Fluid Axisymmetric Z-Pinch

Pinch radius $R = 12.5 R_{gi}$, Perturbation wave length $L = 50 R_{gi}$

1 period shown

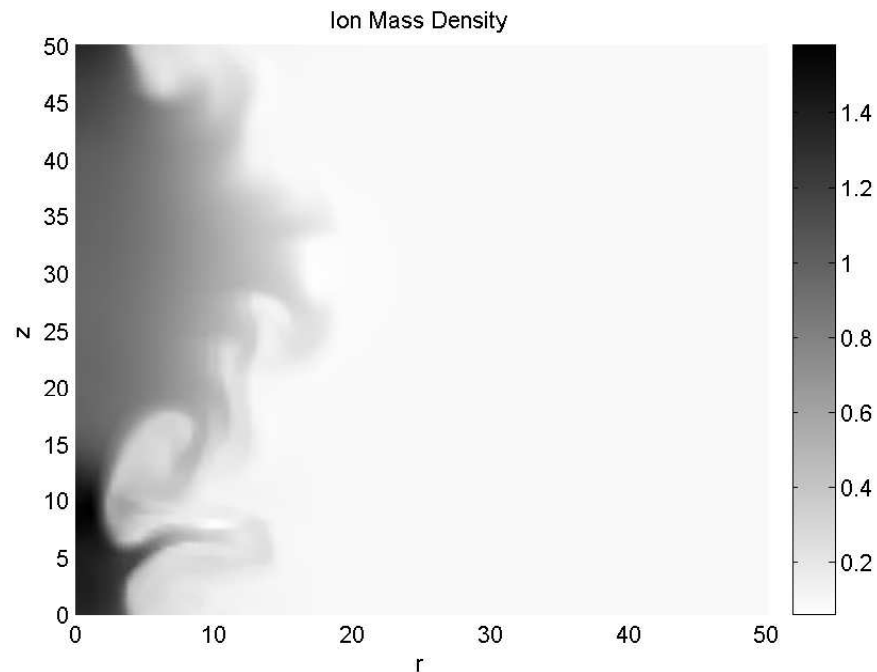


Figure 4: Ion mass density plot after $5\tau_A$. The $L = 50 R_{gi}$ perturbation grows into the non-linear regime. A higher wave number instability is nonlinearly coupled to the initial perturbation and also develops.

Full Two-Fluid Axisymmetric Z-Pinch

Pinch radius $R = 12.5 R_{gi}$, Perturbation wave length $L = 25 R_{gi}$
2 periods shown

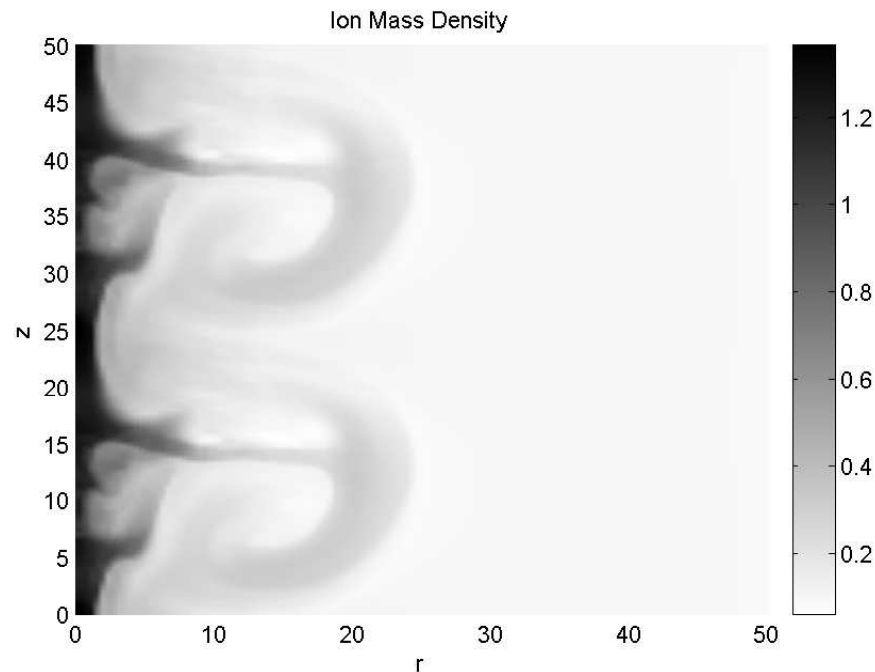


Figure 5: Ion mass density plot after $5\tau_A$. As expected, the $L = 25 R_{gi}$ perturbation grows faster than the $L = 50 R_{gi}$ perturbation - however earlier in time the $L = 25 R_{gi}$ looks very similar to the $L = 50 R_{gi}$ solution.

Full Two-Fluid Axisymmetric Z-Pinch

Pinch radius $R = 2.5 R_{gi}$

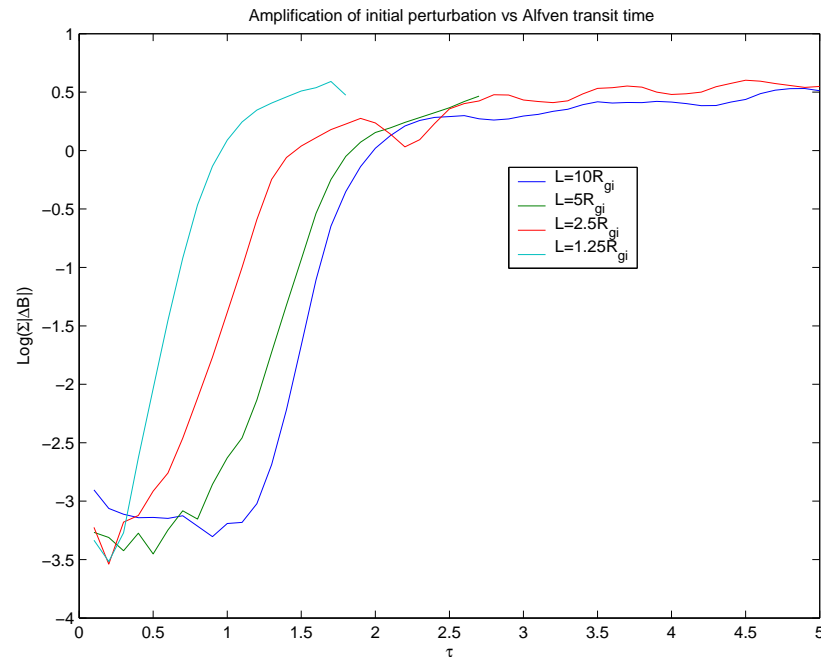


Figure 6: Plots of the growth in the perturbed magnetic field vs time normalized by the Alfvén transit time across the radius. The Z-pinch has radius $R = 2.5 R_{gi}$ and plots are shown for various wavelength perturbations L . The growth occurs faster than MHD time and is associated with an electron flow velocity greater than the ion sound speed.

Full Two-Fluid Axisymmetric Z-Pinch

Pinch radius $R = 2.5 R_{gi}$, Perturbation wave length $L = 10 R_{gi}$
1 period shown

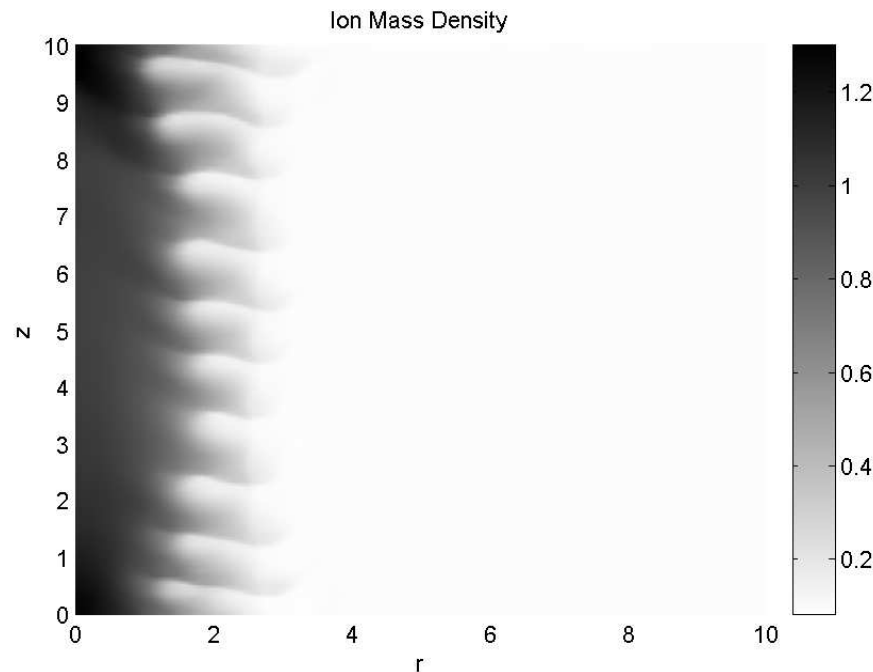


Figure 7: Ion mass density plot after $2\tau_A$. Despite the fact that the solution is initialized with an $L = 10 R_{gi}$ perturbation, waves of length $1 R_{gi}$ develop and grow faster. Shocks develop in the ion fluid indicating that an electron instability is coupled to the ions

Full Two-Fluid Axisymmetric Z-Pinch

Pinch radius $R = 2.5 R_{gi}$, Perturbation wave length $L = 5 R_{gi}$
2 periods shown

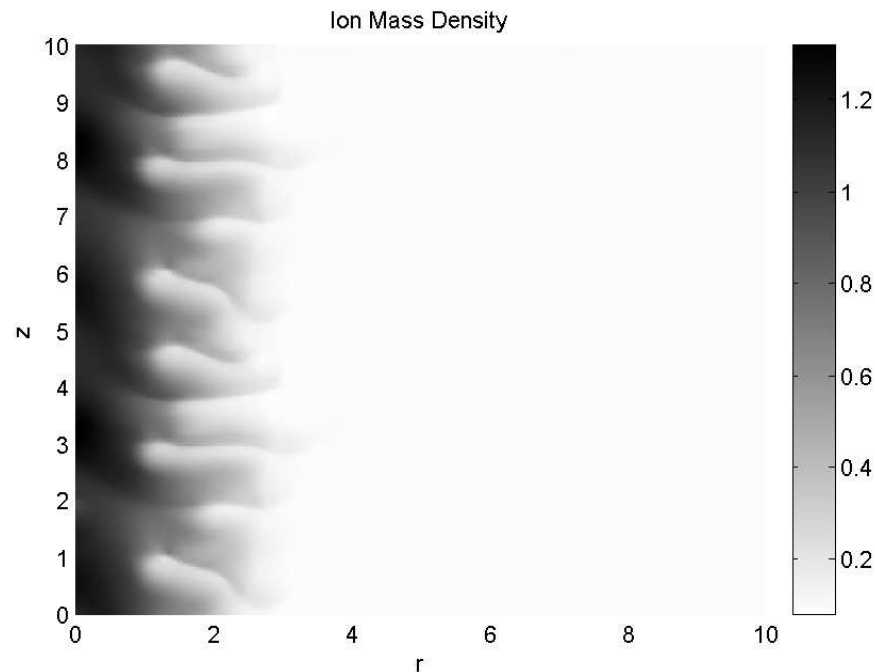


Figure 8: Ion mass density plot after $2\tau_A$. When the initial perturbation wave length is changed to $L = 5 R_{gi}$, the same short wave length $L = 1 R_{gi}$ develops and dominates the non-linear dynamics.

k	$R = 2.5 R_{gi}$	$R = 7.5 R_{gi}$	$R = 12.5 R_{gi}$
1	4.8	1.2	1.1
2	4.0	1.7	1.6
3	3.7	2.3	2.1
4	5.7	2.8	2.5

Table 1: Comparison of growth rates for various pinch radii given mode k. Notice that for pinch radii significantly larger than the ion Larmor radii, MHD growth rates dominate the solution. For pinch radii on the order of the ion Larmor radius it's believed drift instabilities, possibly the drift sausage instability, dominates the growth and development of the non-linear solution.

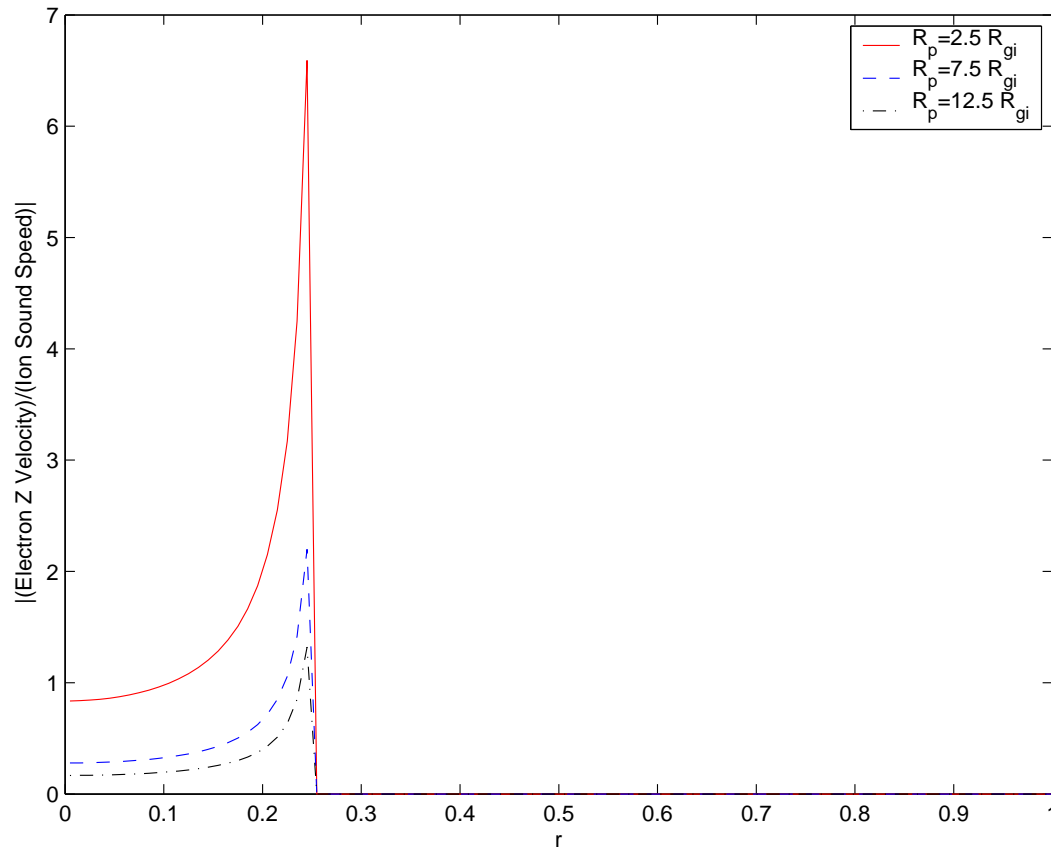


Figure 9: Plot of initial $M_{j e}$ (electrons z velocity/ion acoustic speed) vs radial position for three axisymmetric problems. The smaller the pinch radius in ion Larmor radii the greater the electron z velocity compared to the ion acoustic speed. In particular, shocks develop when a significant portion of the pinch has $M_{j e} > 1$ as in the case $R_p = 2.5 R_{g i}$

Full Two-Fluid Axisymmetric Z-Pinch

For simulations with pinch radii several ion Larmor radii, satisfying a condition where the electron drift velocity is typically less than the ion acoustic velocity, the solution behaves like an MHD solution and the initialized perturbations are the fastest growing mode.

When the typical electron drift velocity is greater than the ion acoustic speed (which corresponds to a current layer less than a few ion Larmor radii) a higher mode instability develops and shock waves form in the ion fluid. These shock waves may be driven by a drift sausage instability (DSI) which is a long wavelength relative to the lower hybrid drift instability. Also, the instability seems fairly robust, even though the solutions presented are rather extreme in their velocity profiles, we have observed the same instability in other Z-pinch simulations as well as theta pinches and electromagnetic explosions where a thin current layer develops at the shock front.

3D Full Two-Fluid Z-Pinch

3D simulations of a Z-pinch have been performed at low resolution and results are shown in the following slides. Due to the computational time required, a grid refinement study has not been performed. The simulations do show the growth of kink and sausage instabilities. Conducting walls are used on a general structured multi-block mesh.

3D Full Two-Fluid Z-Pinch

Pinch radius $R = 2.5 R_{gi}$

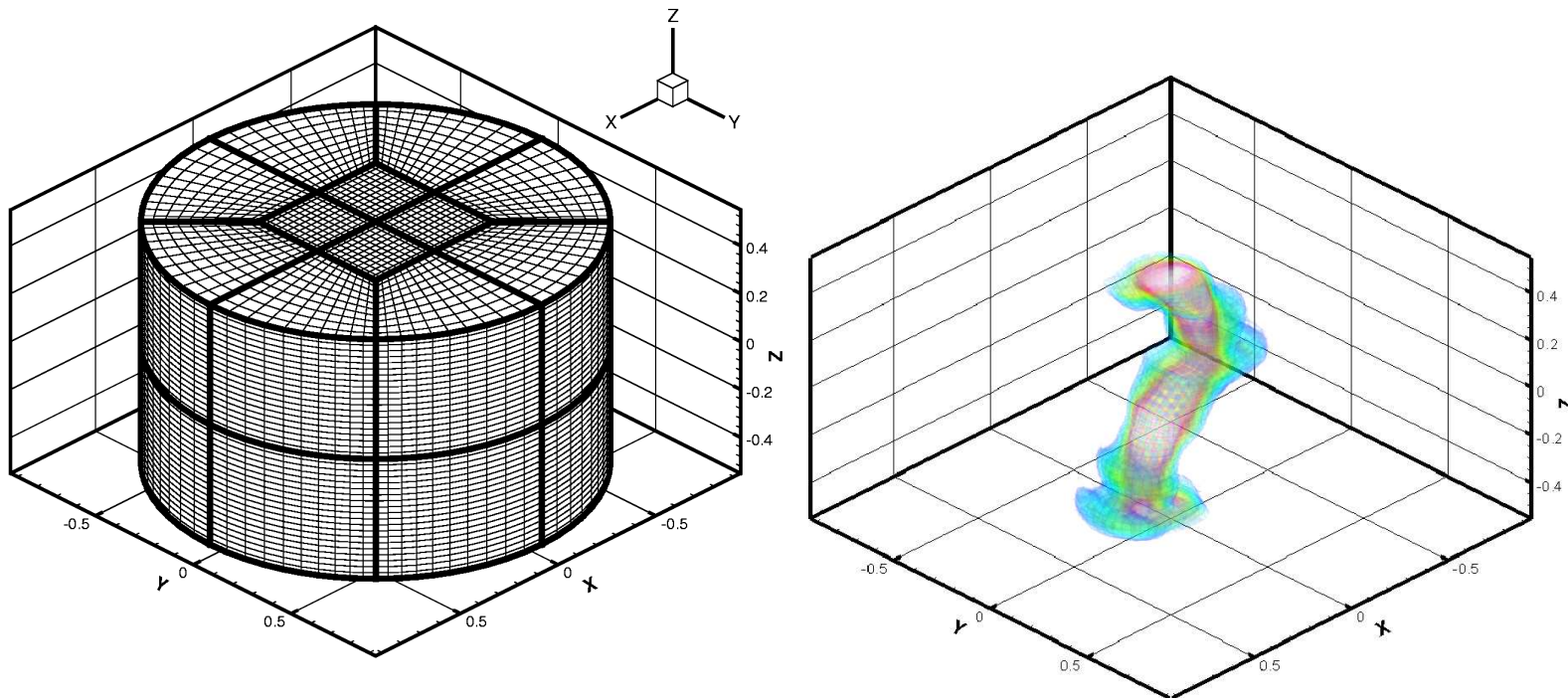


Figure 10: Grid used in 3D Z-pinch simulations and ion pressure profile at $4.125\tau_A$. Development of a kink instability in a 3D Z-pinch using the 2nd order discontinuous Galerkin method with 3rd order Runge-Kutta time stepping.

3D Full Two-Fluid Z-Pinch

Pinch radius $R = 2.5 R_{gi}$

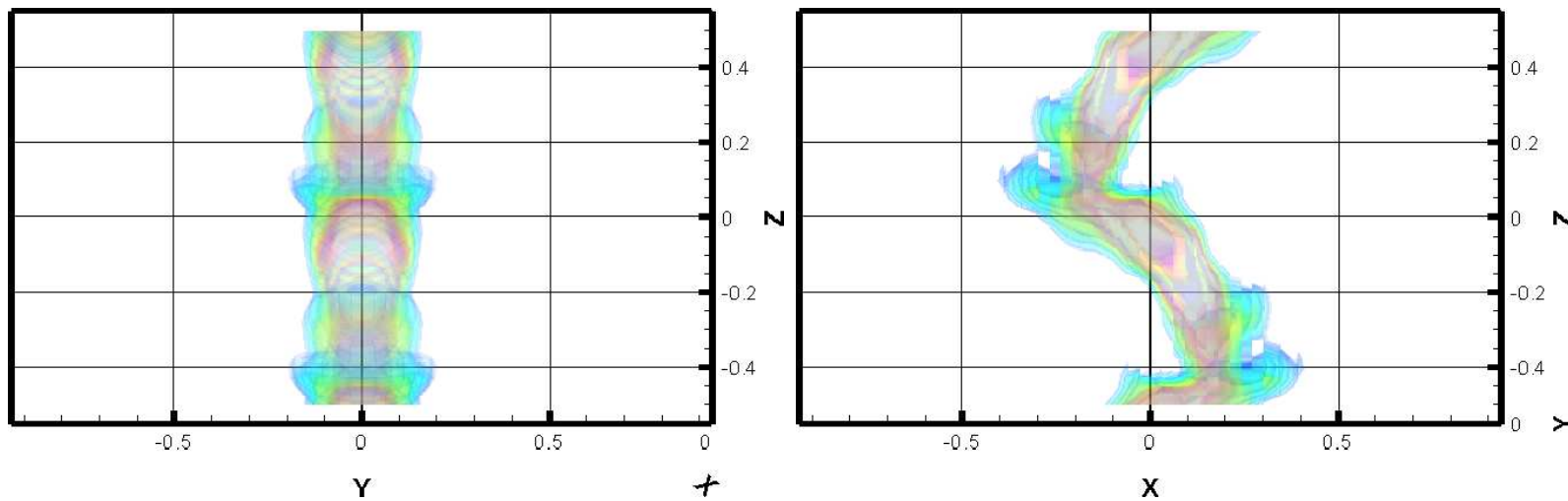


Figure 11: XZ Ion pressure profile at $t = 4.125\tau_A$. Edge views of the kink instability shown in the previous slide. Also notice that a sausage instability develops in the YZ plot.

Conclusion

- An algorithm for the two-fluid plasma model that uses the discontinuous Galerkin method has been developed.
- The method is tested against GEM challenge collisionless reconnection simulations.
- Axisymmetric version of the algorithm has been used in a study of the two-fluid Z-pinch.
- Short wavelength (drift sausage?) instability develop in a Z-pinch when the electron drift speed is greater than the ion sound speed.

References

- [1] J. Birn and et al., *Geospace environmental modeling (gem) magnetic reconnection challenge*, Journal of Geophysical Research **106** (2001), no. A3, 3715–3719.
- [2] Bernardo Cockburn and Chi-Wang Shu, *Tvb runge-kutta local projection discontinuous galerkin finite element method for conservation laws ii: General framework*, Mathematics of Computation **52** (1989), 411–435.
- [3] _____, *The runge-kutta discontinuous galerkin method for conservation laws v: Multidimensional systems*, Journal of Computational Physics **141** (1998), 199–224.
- [4] Bo nan Jiang, Jie Wu, and L. A. Povinelli, *The origin of spurious solutions in computational electromagnetics*, Journal Of Computational Physics **125** (1996), 104–123.
- [5] M. A. Shay, J. F. Drake, B. N. Rogers, and R. E. Denton, *Alfvénic collisionless magnetic reconnection and the hall term*, Journal of Geophysical Research **106** (2001), 3759–3772.